

Fractional Chern insulator candidate in twisted bilayer checkerboard lattice

Jia-Zheng Ma,¹ Rui-Zhen Huang,² Guo-Yi Zhu,³ Ji-Yao Chen,^{1,*} and Dao-Xin Yao^{1,†}

¹*Guangdong Provincial Key Laboratory of Magnetoelectric Physics and Devices, State Key Laboratory of Optoelectronic Materials and Technologies, Center for Neutron Science and Technology, School of Physics, Sun Yat-sen University, Guangzhou, 510275, China*

²*Department of Physics and Astronomy, University of Ghent, 9000 Ghent, Belgium*

³*Institute for Theoretical Physics, University of Cologne, Zùlpicher Straße 77, 50937 Cologne, Germany*

We investigate a fractional Chern insulator (FCI) candidate arising from Moiré bands with higher Chern number $C = 2$ on a magic angle twisted bilayer checkerboard lattice (MATBCB). There are two nearly flat low lying bands in the single particle energy spectrum under the first magic angle $\phi \approx 1.608^\circ$ and chiral limit. We find MATBCB hosts a nearly uniform Berry curvature distribution and exhibits tiny violation of quantum geometric trace condition in the first moiré Brillouin Zone (mBZ), indicating that there is a nearly ideal quantum geometry in MATBCB in single particle level. Turning on projected Coulomb interactions, we perform exact diagonalization and find a ten-fold ground state quasi-degeneracy in many body energy spectrum with filling fraction $\nu = 1/5$. The ten-fold quasi-degenerate ground states further show spectra flow under flux pumping. By diagnosing the particle entanglement spectrum (PES) of the ground states, we obtain a clear PES gap and quasi-hole state counting consistent with Halperin spin singlet generalized Pauli principle, suggesting that a $C = 2$ abelian fractional Chern insulator is realized in this system.

I. INTRODUCTION

Fractional Chern insulator (FCI) is a lattice enriched version of fractional quantum hall effect (FQHE). It is believed to be realizable under weak magnetic field or even with zero external magnetic field, and has attracted many interest in both theoretical and experimental communities. An important potential application of FCI is topological quantum computation [1, 2]. The existence of FCI phase was predicted by theory decades ago [3–8]. Recently, several experiments have realized the fractional quantum anomalous hall effect (FQAHE) in material system including twisted MoTe_2 system [9–11] and rhombohedral pentalayer graphene (R5G) [12]. FQAHE can be considered as a phenomenon in zero magnetic field FCI phase with fractional anomalous hall conductivity. Twisted MoTe_2 and R5G become better system than twisted bilayer graphene (TBG) in realizing FCI phase, since the FCI phase in TBG needs weak external magnetic field to make it more stable [13].

These experiments have raised a great interest among theorists. Several theories have been proposed to interpret the FQAHE (zero magnetic field FCI) in MoTe_2 [14–23] and R5G [24–30]. Besides gapped phases, gapless phases beyond FQAHE, e.g., the composite fermi liquid phase, have also been found [31]. However, the experiments mentioned above all seem to focus on fractional filling $C = 1$ Chern band which has well known lowest Landau level (LLL) correspondence. When the topological flat band host a higher Chern number, its potential FCI phase will not have a naive LLL correspondence [32–36]. What is more attracting, it is possible to realize non-abelian FCI phase [20, 32, 37–48] in fractionally filled flat band with higher Chern number, which could be a building block for fault-tolerant quantum computation.

Motivated by above progress, it is valuable to search for higher Chern number FCI phase in real material or artificial system. In this manuscript, we theoretically study a $C = 2$ abelian FCI candidate in magic angle twisted bilayer checkerboard (MATBCB) lattice model [49] with fractional filling $\nu = 1/5$ of the lowest single particle conductive band. By using exact diagonalization (ED) in momentum space, we find there is a ten-fold ground state quasi-degeneracy in the many-body energy spectrum and the spectrum flow under adiabatic flux inserting. These ten-fold low energy states are the topological ground state candidates for putative $C = 2$ FCI phase. From the perspective of many-body entanglement, we study the particle entanglement spectrum (PES) of these ten-fold ground states density matrix. We find that the quasi-hole counting under PES gap obeys the Halperin spin singlet generalized Pauli principle (GPP), which is a smoking gun evidence for the existence of $C = 2$ FCI phase. This higher Chern number FCI phase may be realized in artificial quantum simulator such as Rydberg atom array [50], twisted optical lattice [51–54], circuit QED system [55]. Up to now, we have noticed that several works have studied TBCB flat band [49, 56], or similar system like twisted square lattice [57–60], twisted FeSe [61], strained moiré lattice with quadratic dispersion [62], and square lattice moiré heterostructure [63].

This manuscript is organized as follows: In section II, we briefly review the single particle Bistritzer-MacDonald (BM) like model of TBCB and derive the topologically non-trivial two lowest flat bands with higher Chern number $C = \pm 2$. In section III, we examine the single particle quantum geometry indicator for MATBCB flat band and check if it is suitable for MATBCB to host FCI phase. Then in section IV, we turn to the flat band projected interacting many-body model of MATBCB with filling fraction $\nu = 1/5$ to reveal the potentially topological many-body ground states and their spectrum flow under adiabatic flux inserting. In section V, we further present the PES of putative topological ground state density matrix and show the quasi-hole statistics. The quasi-

* chenjiy3@mail.sysu.edu.cn

† yaodaoy@mail.sysu.edu.cn

hole counting obeys the Halperin spin singlet GPP, indicating the phase in TBCB under magic angle and chiral limit is a FCI instead of a CDW or other competing phases. In section VI, we conclude and discuss further directions with large-scale numerical approaches for hunting FCI in moiré system with higher Chern number.

II. SINGLE PARTICLE MOIRÉ BAND STRUCTURE OF MATBCB

In this section we solve the Moiré Hamiltonian (free fermion hopping in momentum space) of MATBCB and show the flat band structure, as well as the non-trivial Chern number. To clarify, in the following we will use lower case k to label the single particle momentum while the upper case K denotes the many body momentum or total momentum. The two dimensional single particle wave vector is defined as $\mathbf{k} = (k_x, k_y)$. The Greek symbol $\kappa = w_{AA}/w_{AB}$ represents chiral ratio to be introduced later. The Moiré Hamiltonian for a given momentum $H(k_x, k_y)$ expressed in reciprocal lattice basis is shown in Eq. (1):

$$H = \sum_{k, q_{i,b}, q_{i,t}} h(k, q_{i,b}, q_{i,t}) + \sum_{k, (q_{j,t}, q_{i,b})} \begin{pmatrix} c_{k,q_{j,t}}^\dagger & c_{k,q_{i,b}}^\dagger \end{pmatrix} \begin{pmatrix} 0 & T_{q_{j,t}, q_{i,b}} \\ T_{q_{j,t}, q_{i,b}}^\dagger & 0 \end{pmatrix} \begin{pmatrix} c_{k,q_{j,t}} \\ c_{k,q_{i,b}} \end{pmatrix}, \quad (1)$$

where we have denoted

$$h(k, q_b, q_t) = \begin{pmatrix} c_{k,q_t}^\dagger & c_{k,q_b}^\dagger \end{pmatrix} \begin{pmatrix} H_0^{\phi/2}(k - q_t) & T_{q_t, q_b} \\ T_{q_t, q_b}^\dagger & H_0^{-\phi/2}(k - q_b) \end{pmatrix} \begin{pmatrix} c_{k,q_t} \\ c_{k,q_b} \end{pmatrix}, \quad (2)$$

with

$$H_0^\phi(k) = 2t' \cos(k_x - k_y)(\cos \phi \sigma_y + \sin \phi \sigma_x) + 4t \cos\left(\frac{k_x + \pi}{2}\right) \cos\left(\frac{k_y + \pi}{2}\right)(\cos \phi \sigma_x - \sin \phi \sigma_y) + \Delta \sigma_z, \quad (3)$$

and

$$T_{q_t, q_b} = (w_{AA}I + w_{AB}\sigma_x)[\delta(q_t^x = q_b^x + \frac{k_\phi}{\sqrt{2}})\delta(q_t^y = q_b^y + \frac{k_\phi}{\sqrt{2}}) + \delta(q_t^x = q_b^x - \frac{k_\phi}{\sqrt{2}})\delta(q_t^y = q_b^y - \frac{k_\phi}{\sqrt{2}})] + (w_{AA}I - w_{AB}\sigma_x)[\delta(q_t^x = q_b^x + \frac{k_\phi}{\sqrt{2}})\delta(q_t^y = q_b^y - \frac{k_\phi}{\sqrt{2}}) + \delta(q_t^x = q_b^x - \frac{k_\phi}{\sqrt{2}})\delta(q_t^y = q_b^y + \frac{k_\phi}{\sqrt{2}})], \quad (4)$$

Exact diagonalizing this Hamiltonian gives rise to the Moire band structure $\epsilon(k_x, k_y)$ and the Bloch orbitals $u(k_x, k_y)$. The band structure is shown in Fig. 1.

Here H_0 is the Hamiltonian for monolayer checkboard lattice with quadratic dispersion. T_{q_t, q_b} is the interlayer

coupling between quadratic nodes q_t, q_b . T_{q_t, q_b} includes intra-mBZ term and inter-mBZ term. $h(k, q_b, q_t)$ is the Hamiltonian within mBZ. The TBCB parameters include intra-sublattice hopping t' and inter-sublattice hopping t , interlayer coupling in AA region w_{AA} and the AB region counterpart w_{AB} . In Eq. (4), $k_\phi = \frac{2\sqrt{2}\pi}{a} \sin(\phi/2)$ is the distance between adjacent quadratic points from each layer in momentum space and a is the lattice constant for monolayer. Here we restrict the parameters at the first magic angle $\phi = 1.608^\circ$, chiral limit $t' = t/2 = 500$ meV, $w_{AB} = 2.05$ meV, $w_{AA} = 0$ as suggested in Ref. [49]. In addition, we have added a sublattice mass term $\Delta \sigma_z$ compared with [49] to make many body computation simpler in the next section. The representation space of flat band Bloch orbital is the direct product of reciprocal point, sublattice and layer space. As shown in Fig. 1, red points represent the reciprocal lattice of bottom layer and blue points are the counterpart for top layer.

To elucidate the topological nature of the flat band, we evaluate the non-contractible Wilson loop circumventing the mBZ in x direction, defining $|u_\alpha(\mathbf{k})\rangle$ as the periodic part of Bloch function at band α . One has the following overlap matrix and Wilson loop:

$$\begin{aligned} [O(k_x, k_y)]_{\alpha\beta} &= \langle u_\alpha(k_x, k_y) | u_\beta(k_x + dk_x, k_y) \rangle, \\ dk_x &= \frac{2\pi}{N_x}, \quad \alpha, \beta = 1, 2. \\ W(k_y) &= \left[\prod_{n_x=1}^{N_x-1} O\left(k_x = \frac{2\pi}{N_x}(n_x - \frac{N_x+1}{2}), k_y\right) \right] O'(k_y), \quad (5) \\ [O'(k_y)]_{\alpha\beta} &= \sum_{G_x, G_y, \tau, \mu} \langle u_\alpha(k_x = \frac{\pi(N_x-1)}{N_x}, k_y) | G_x, G_y, \tau, \mu \rangle \\ &\langle G_x - 2\pi, G_y, \tau, \mu | u_\beta(k_x = -\frac{\pi(N_x-1)}{N_x}, k_y) \rangle. \end{aligned}$$

From which we extract the global Berry flux threaded into the compactified mBZ towards the k_y direction. The Berry flux for the quasi-degenerate two flat bands are shown in Fig. 2(a), which means the flat bands carry Chern numbers $C = \pm 2$ respectively.

The eigenvalues for matrix $W(k_y)$ in Eq. (5) are just the winding phases of the polarization. The eigenfunction of Hamiltonian Eq. (1) under reciprocal point, sublattice, layer direct product basis is labeled by $\langle G_x, G_y, \tau, \mu | u_\alpha(k_x, k_y) \rangle$, and $G = (G_x, G_y)$ is the reciprocal vector. α, τ, μ represent band, sublattice and layer respectively. The complete relation is $\sum_{G_x, G_y, \tau, \mu} |G_x, G_y, \tau, \mu\rangle \langle G_x, G_y, \tau, \mu| = I$. When the winding link goes across the boundary of the first mBZ, one should shift the component of the Bloch wavefunction by a primitive reciprocal vector in x direction to ensure that the overlap O' is still a first-order infinitesimal matrix. It corresponds to inserting the embedding matrix [49, 64, 65] like Eq. (5). The k space embedding matrix has its real space counterpart in Ref. [66]. For a given k_y , in principle one can start from arbitrary k_x to get the winding $W'(k_x, k_y)$ as long as inserting embedding matrix when crossing the mBZ boundary. One can easily prove that $W(k_y)$ and $W'(k_x, k_y)$ share the trace and determinant. So the eigenvalues for $W(k_y)$ and $W'(k_x, k_y)$ are

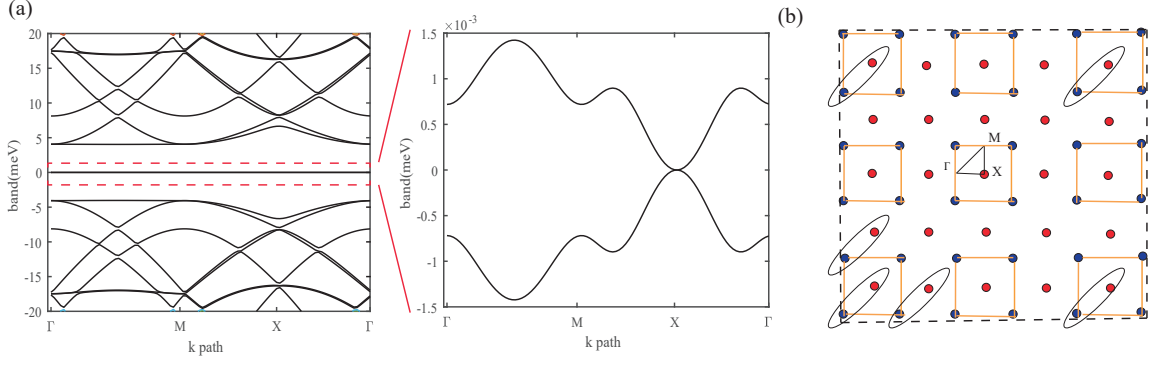


FIG. 1. (a) The single particle Moiré band structure along high symmetry path in the first mBZ and the zoomed in figure of the lowest two bands. One can see that the bandwidth at the first magic angle $\phi \approx 1.608^\circ$ and chiral limit $\kappa = w_{AA}/w_{AB} = 0$ is about 1.5×10^{-3} meV. There is a quadratic band touching at X point which reflects the nature of tight binding checkboard lattice model dispersion when $\Delta = 0$. The number of k points in the high symmetry path is 100 and the size of quadratic node array is 25×25 in single particle calculation. (b) The scheme of quadratic gapless node array in momentum space for TBCB, which is similar to Dirac cone in TBG. Blue ones represent the top layer nodes and red ones are bottom layer nodes. The yellow square is one of the choice of the first mBZ. Moiré tunneling will occur between each pair of the nearest nodes. The elliptic can be considered as the minimal unit in this array.

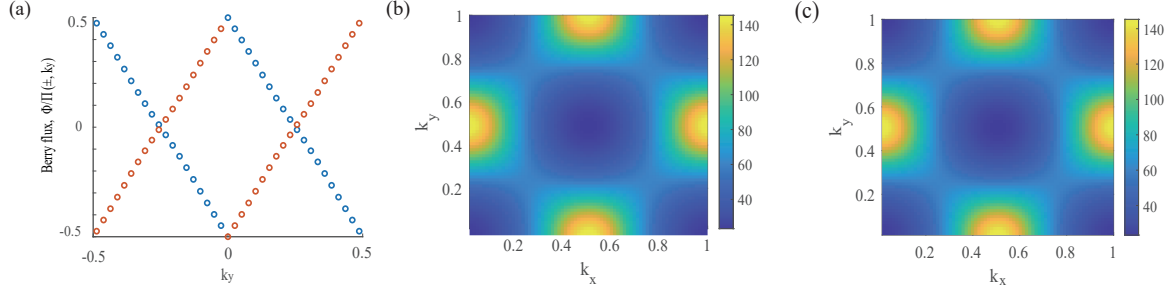


FIG. 2. (a) The Wilson loop winding of the lowest two flat bands near half filling. Since the single particle band is gapless at X, the Wilson loop is a 2×2 matrix. The windings are corresponding to the two eigenvalues of the Wilson loop. One can read out the Chern number $C = \pm 2$. From the variation speed of the winding, one can believe that the Berry curvature distribution is uniform enough to host a FCI phase. (b) The Berry curvature given by Eq. (10). The k point density in the first mBZ is 74×74 . (c) The trace of quantum metric in the first mBZ using the same k point density. It almost has the same distribution with Berry curvature, which implies the single particle flat band Bloch function is close to a holomorphic function about $k = k_x + ik_y$, and ideal trace condition violation. The range of momentum k_x, k_y are the same $[0, 2\pi]$ for (b) and (c).

the same for arbitrary k_x . However, the eigenvectors for $W(k_y)$ and $W'(k_x, k_y)$ are generally different. These eigenvectors can be related by wilson line like Ref. [66].

Importantly, when $N_x \rightarrow \infty, dk_x \rightarrow 0$, $O(k_x, k_y)$ and $W(k_y)$ are unitary matrices. Nevertheless in realistic numerical implementation, N_x is finite so $O(k_x, k_y)$ will be a non-unitary matrix. In order to get unitary $W(k_y)$ and its pure phase eigenvalues, one has to extract the unitary part of $O(k_x, k_y)$. Available strategy can be singular value decomposition (SVD) [66]

$$O(\mathbf{k}) = U(\mathbf{k})S(\mathbf{k})V^\dagger(\mathbf{k}), \quad \tilde{O}(\mathbf{k}) = U(\mathbf{k})V^\dagger(\mathbf{k}), \quad (6)$$

or polar decomposition [67]:

$$\begin{aligned} O(\mathbf{k}) &= P(\mathbf{k})R(\mathbf{k}), \quad R(\mathbf{k}) = \sqrt{O^\dagger(\mathbf{k})O(\mathbf{k})}, \\ P(\mathbf{k}) &= \tilde{O}(\mathbf{k}) = O(\mathbf{k})R^{-1}(\mathbf{k}) = O^{1/2}(\mathbf{k})[O^\dagger(\mathbf{k})]^{-1/2}. \end{aligned} \quad (7)$$

Here we denote the unitary part of $O(k_x, k_y)$ as $\tilde{O}(k_x, k_y)$. Accordingly, $\tilde{W}(k_y)$ will also be a unitary matrix. With these tricks, one can go back and inspect the single particle energy spectrum and Wilson loop. In Fig. 1, we set the sublattice staggered potential $\Delta = 0$. And we find that the lowest quadratic flat bands in MATBCB are about 1.5×10^{-3} meV wide. From the Wilson loop winding of flat bands shown in 2(a), one can see that there is almost uniform winding over the mBZ. It is reminiscent that MATBCB may satisfy the ideal quantum geometry condition well, which is suitable for hosting FCI phase.

Up to now we have a preliminary picture of MATBCB in single particle level including single particle band and Wilson loop winding. In the next section, we will use quantum geometry indicators to inspect if MATBCB is favor to host FCI phase more carefully.

III. QUANTUM GEOMETRY INDICATORS FOR FRACTIONAL CHERN INSULATOR

In this section we compute the distribution of Berry curvature and the quantum geometry tensor in mBZ, to inspect the quantitative difference of our flat band Bloch orbitals from the lowest Landau levels (LLL). The quantum geometry indicators for FCI phase in single particle level include [43, 68]:

1. The bandwidth need to be narrow enough to suppress the kinetic term. It should be much more narrow than single particle excitation gap and interaction energy scale.
2. The standard deviation of Berry curvature over the first mBZ $\sigma[\eta] = [\frac{1}{2\pi} \int d^2k (F(\mathbf{k}) - \bar{F})^2]^{1/2}$ should be as small as possible. Here $F(\mathbf{k})$ is Berry curvature while $\bar{F} = 2\pi C/A$ represents averaged Berry curvature. C is Chern number and A is the area of mBZ. The uniform Berry curvature is good to host FCI which corresponds to LLL.
3. The trace condition violation $T[\eta] = \frac{1}{2\pi} \int d^2k (Tr(g) - |F|)$. g is quantum metric (Fubini-Study metric) which will be introduced in details later. $T[\eta]$ measures the deviation between flat band Bloch wave function and holomorphic function about $k = k_x + ik_y$. To host the FCI phase, this violation is also required to be as small as possible.

In fact, there is still some subtlety when applying quantum geometry indicator to higher Chern number band, for which a recent generalization can be found in Ref. [43, 69]. Here for simplicity, our strategy is to transform the higher Chern number problem to familiar $C = 1$ case. Fortunately, several recent works have shown that ideal higher Chern band can be decomposed into a set of $C = 1$ ideal Chern bands [70, 71] under certain condition. Specially, when the Berry curvature of $C > 1$ Chern band satisfies $F(\mathbf{k}) = F(\mathbf{k} + \mathbf{Q})$ with \mathbf{Q} being some translation symmetry broken vector, the set of decomposed $C = 1$ ideal Chern bands can form orthogonal basis. That means these $C = 1$ bands can be independently filled. So the $C = 1$ quantum geometry indicators can be used as usual. In our MATBCB case, $\mathbf{Q} = (G_1/2, G_2/2)$. One can see this point later in detail. A more general FCI indicator may be the so-called vortexability [72, 73], which we leave for future work.

In our two flat bands subspace, we define the multiband version infinitesimal distance between adjacent Bloch states and the quantum geometry tensor as follows:

$$ds^2 = \left| \sum_n \langle u_{\mathbf{k}}^a | u_{\mathbf{k}}^n \rangle \langle u_{\mathbf{k}}^n | u_{\mathbf{k}}^b \rangle - \sum_n \langle u_{\mathbf{k}+d\mathbf{k}}^a | u_{\mathbf{k}}^n \rangle \langle u_{\mathbf{k}}^n | u_{\mathbf{k}+d\mathbf{k}}^b \rangle \right| \approx \eta_{\mu\nu}^{ab} dk^\mu dk^\nu,$$

$$\eta_{\mu\nu}^{ab} = \langle \partial_{k^\mu} u_{\mathbf{k}}^a | (I - \sum_n |u_{\mathbf{k}}^n\rangle \langle u_{\mathbf{k}}^n|) | \partial_{k^\nu} u_{\mathbf{k}}^b \rangle = \langle \partial_{k^\mu} u_{\mathbf{k}}^a | (I - P(\mathbf{k})) | \partial_{k^\nu} u_{\mathbf{k}}^b \rangle$$
(8)

Here the repeated index μ, ν means summing over. $P(\mathbf{k})$ is the projection operator of two band subspace. The summation of

n run over the 2 band subspace. μ, ν label the momentum component $\{k_x, k_y\}$. a, b label the band index. η is the quantum geometry tensor (QGT) [43, 68]. Its real part and imaginary part define the quantum metric and Berry curvature respectively, see Eq. (9). We can see that QGT contains more information than Wilson loop or Berry curvature.

$$g_{\mu\nu}^{ab} = \frac{1}{2}(\eta_{\mu\nu}^{ab} + \eta_{\nu\mu}^{ab}), \quad F^{ab} = i\epsilon^{\mu\nu} \eta_{\mu\nu}^{ab}. \quad (9)$$

For FCI phase, we mainly concern the Berry curvature F and trace of quantum metric $Tr(g)$. In practice, one can use the following Wilson loop formalism Eq. (10) to get $F, Tr(g)$ simultaneously and accurately [43]. For the mBZ (torus T^2), there is no need to fix the gauge [74]. Compared with simply using Eq. (8), Eq. (10) can better capture the non-linear character in F and $Tr(g)$ especially when the \mathbf{k} point is near the branch cut of Berry phase or the boundary of mBZ. Here we assume $dk_x = dk_y$.

$$[U_r(\mathbf{k})]_{ab} = \langle u_a(\mathbf{k}) | u_b(\mathbf{k} + d\mathbf{k}_r) \rangle, \quad r = x, y,$$

$$W(\mathbf{k}) = [U_y(\mathbf{k})]^{-1} [U_x(\mathbf{k} + dk_x)]^{-1} U_y(\mathbf{k} + dk_x) U_x(\mathbf{k})$$

$$= \exp(-g_{k_x k_x} dk_x^2 - g_{k_y k_y} dk_y^2) \exp(iF dk_x dk_y),$$

$$W = USV^\dagger, \quad \exp(iF dk_x dk_y) = UV^\dagger, \quad S = \exp(-Tr(g) dk_x^2),$$

$$C = \frac{1}{2\pi} \int_{mBZ} d^2k Tr(F) = \frac{1}{2\pi i} \int_{mBZ} Tr(\ln(W(\mathbf{k})))$$

$$= \frac{1}{2\pi i} \int_{mBZ} \ln(\det(W(\mathbf{k}))),$$

$$F = \frac{\mathbf{Im}(\ln(W))}{dk_x dk_y}, \quad Tr(g) = -\frac{\mathbf{Re}(\ln(W))}{dk_x^2}. \quad (10)$$

From Fig. 2, one can see that Berry curvature of $C = +2$ band (Wilson eigenvalue) and the trace of quantum metric are consistent, which means the ideal trace condition violation condition is well satisfied. The profile of Berry curvature is similar to the result given by Ref. [75], which indicates topological heavy fermion is also a potential competing phase. More importantly, one can see that the Berry curvature host the symmetry $F(\mathbf{k}) = F(\mathbf{k} + \mathbf{Q})$, $\mathbf{Q} = (G_1/2, G_2/2)$. That means the $C = 2$ band can be orthogonally decomposed into two $C = 1$ bands. Therefore the original quantum geometry indicator for $C = 1$ case is still valid in our $C = 2$ MATBCB system. For MATBCB, we summarize the quantum geometry indicators as follow:

1. The single body bandwidth is $W = 1.5 \times 10^{-3}$ meV.
2. The standard deviation of Berry curvature is $\sigma[\eta] = 6.0579$.
3. The trace condition violation is $T[\eta] = 1.6357 \times 10^{-7}$.

Compared with MATBG [13, 68], MATBCB has more ideal bandwidth and trace condition violation but slightly worse Berry curvature deviation. We note that some recent works have proposed the concept of higher Berry curvature [76–78], which may develop to many-body version

quantum geometry. Also the trace condition deviation can be generalized to local momentum \mathbf{k} version [79]. How to apply them to moiré system will be an interesting problem.

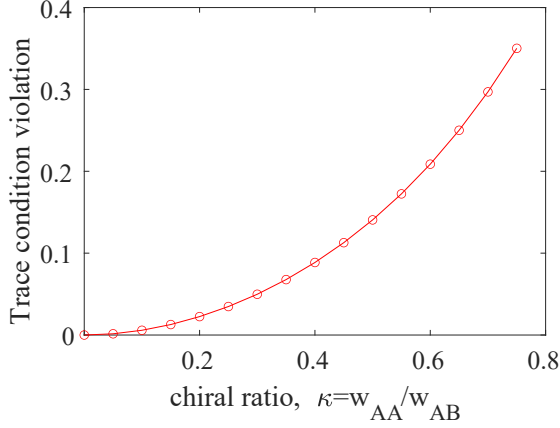


FIG. 3. The variation of trace condition violation $T[\eta]$ over chiral ratio κ under $\Delta = 1meV$ case. One can read out that $T[\eta]$ is monotonically increasing with κ , which indicates that non-zero chiral ratio can induce the instability of putative FCI phase.

For the non-ideal case, one can consider the non-chiral limit with non-zero w_{AA} . The result is shown in Fig. 3. We inspect the key indicator trace condition violation $T[\eta]$ variation which is directly related to vortexability [72] about chiral ratio κ in single particle level. The $T[\eta]$ is monotonically increasing over κ . Apparently, chiral limit corresponds to the most ideal quantum geometry for TBCB.

To sum up for this section, in single particle level, MATBCB is tend to host $C = 2$ FCI phase according to quantum geometry indicators and higher Chern number ideal band decomposition formalism. However, we still need a many-body interpretation of the FCI candidate in MATBCB in the context of many body ground state degeneracy and entanglement. In the next section we will present a many body picture of putative FCI phase in MATBCB.

IV. MANY-BODY ENERGY SPECTRUM AND SPECTRUM FLOW FOR FCI CANDIDATE

In this section we analyse the corresponding many-body model for MATBCB and solve the low energy spectrum and spectrum flow to see if there is FCI like topological degenerate ground states candidate. For simplicity, we will consider the following projected Coulomb interaction model for topological flat band [49], which is similar to TBG case [64, 65, 80–83]. Strictly speaking, the projection approximation still needs to be improved to consider the renormalization effect from filled bands, like Hartree-Fock approximation (HFA) [26, 68] or perturbation renormalization [25, 84]. More precise modeling will be left for future work. In addition, we set $\Delta = 1meV$ in Eq. (1) from now on to gap out the lowest two flat bands, which means we will only take conductive band

and single valley (K valley) into account for less computation cost. We have numerically checked that when staggered gap is much larger than the single particle flat band width ($\Delta \gg W$), the many body energy is not sensitive to staggered gap Δ .

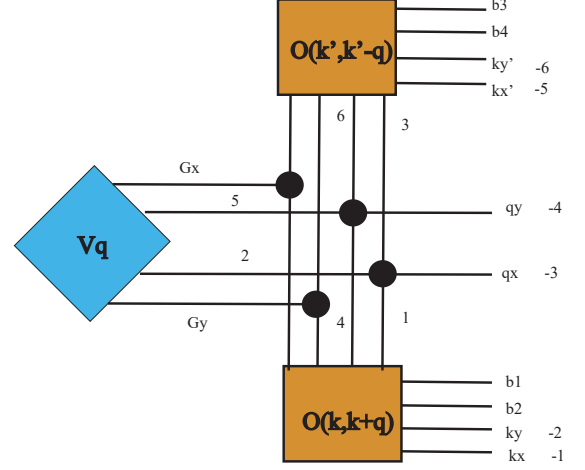


FIG. 4. The tensor form of the projected interaction matrix element. It can be considered as the contraction between bare Coulomb interaction (V_q) and flat band form factor ($O(\mathbf{k}, \mathbf{k} + \mathbf{q})$). Following the convention in tensor network, the legs labelled by negative number are external indices in projected interaction, while legs labelled by positive number are the contracted indices with corresponding ordering. The black dots are higher rank Kronecker tensor. For our case, the band indices are all one dimensional so we will omit them in the following. All the contractions are realized by Neon tensor contractor.

The many body Hamiltonian is as follows (Eq. (11)):

$$H = \sum_{\mathbf{k}, n} \epsilon_{\mathbf{k}, n} C_{\mathbf{k}, n}^\dagger C_{\mathbf{k}, n} + \frac{1}{2A} \sum_{i, j, k, l, \mathbf{k}, \mathbf{k}', \mathbf{q}} V_{i, j, m, l}(\mathbf{k}, \mathbf{k}', \mathbf{q}) (C_{\mathbf{k}+\mathbf{q}, i}^\dagger C_{\mathbf{k}, j} - \bar{\rho}_{\mathbf{q}=0} \delta_{i, j}) (C_{\mathbf{k}'-\mathbf{q}, m}^\dagger C_{\mathbf{k}', l} - \bar{\rho}_{\mathbf{q}=0} \delta_{m, l}), \quad (11)$$

where

$$V_{i, j, m, l}(\mathbf{k}, \mathbf{k}', \mathbf{q}) = \sum_{\mathbf{Q}} V(\mathbf{q} + \mathbf{Q}) O_{i, j}(\mathbf{k}, \mathbf{q}, \mathbf{Q}) O_{m, l}(\mathbf{k}', -\mathbf{q}, -\mathbf{Q}), \quad (12)$$

with

$$O_{i, j}(\mathbf{k}, \mathbf{q}, \mathbf{Q}) = \sum_{\mathbf{G}, \tau, \mu} u_{\mathbf{k}+\mathbf{q}+\mathbf{Q}, i}^*(\mathbf{G}, \tau, \mu) u_{\mathbf{k}, j}(\mathbf{G}, \tau, \mu) = \sum_{\mathbf{G}, \tau, \mu} u_{\mathbf{k}+\mathbf{q}, i}^*(\mathbf{G} - \mathbf{Q}, \tau, \mu) u_{\mathbf{k}, j}(\mathbf{G}, \tau, \mu). \quad (13)$$

Here $\epsilon_{\mathbf{k}, n}$ represents the conductive band single particle energy given by Hamiltonian Eq. (1). This kinetic term will be overwhelmed by interaction near magic angle. The flat band will have well defined Chern number $C = 2$ after gapping out. $C_{\mathbf{k}, n}$ is the flat band fermion annihilation operator, \mathbf{k} labels momentum and n labels band. $A = N_x N_y$ is the normalized area which corresponds to the \mathbf{k} point discretization of the

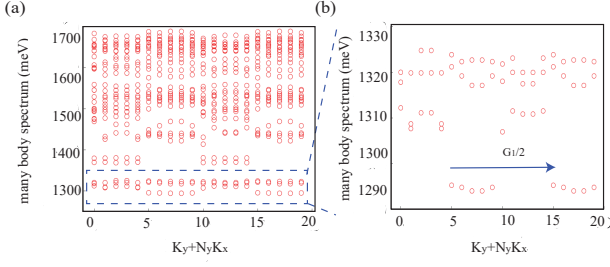


FIG. 5. (a) The many body energy spectrum for $\nu = 1/5$ MATBCB under chiral limit. The discretization of the first mBZ is 4×5 . The number of mBZ is 7×7 which is the size of quadratic nodes array. We will use the same parameters in the following simulation unless specified explanation. (b) The zoomed in of low energy window in (a). One can identify the ground state manifold with GSD=10 at total momentum sector $K = 5, 6 \dots 9$ and $K = 15, 16 \dots 19$. They are approximately related by vector $G_1/2$. The gap between ground state manifold and the higher excitation states is about 12 meV.

first mBZ. In the following, we use the discretization choice of momentum:

$$k_x = \frac{2\pi}{N_x}(0, 1 \dots, N_x - 1), k_y = \frac{2\pi}{N_y}(0, 1 \dots, N_y - 1).$$

$V_{i,j,m,l}(\mathbf{k}, \mathbf{k}', \mathbf{q})$ represents the matrix elements of the projected Coulomb interaction. Since we only consider conductive band, the band indices i, j, m, l are one dimensional and we will omit them after that. The tensor form of $V_{i,j,m,l}(\mathbf{k}, \mathbf{k}', \mathbf{q})$ is shown in Fig. 4. The concrete matrix elements are computed by non tensor contractor [85]. $V(\mathbf{q}) = \frac{2\pi e^2}{\epsilon_r \epsilon_0} \frac{\tanh(|\mathbf{q}|d/2)}{|\mathbf{q}|}$ is the dual gate bare screened Coulomb potential in momentum space. d is the dual gate distance and ϵ_r is the relative dielectric constant. In principle it can be generalized to layer resolved version [66], here for simplification we do not resolve the layer in $V(\mathbf{q})$. $O_{i,j}(\mathbf{k}, \mathbf{q}, \mathbf{Q})$ is the flat band projective form factor. The overlap sums over quadratic reciprocal points \mathbf{G} , sublattice τ , layer μ . The analytical form of the form factor has rich algebraic structure [49, 65]. Numerically, there is phase ambiguity for Bloch function at each \mathbf{k} point. So one has to fix the gauge (the phase difference between each pair of \mathbf{k} points) to make projective interaction matrix element smooth about $\mathbf{k}, \mathbf{k}', \mathbf{q}$. Due to the intrinsic topological non-trivial flat band, the phase discontinuity is unavoidable [33, 67, 86]. One can hide it at the boundary of the first mBZ. The phase of form factor is fixed to $O(\mathbf{k}, \mathbf{q}, \mathbf{Q}) \rightarrow |O| \exp[i \frac{2\pi C}{G_1 G_2} (q_x + Q_x)(q_y + Q_y)]$. When $\mathbf{k} + \mathbf{q}$ goes beyond the first mBZ, one has to pull back it to the first mBZ with reciprocal vector $\tilde{\mathbf{G}}$ and compensate it in the quadratic node array as Fig. 1.

Unlike the integer filling situation whose ground state is almost a Slater determinant [49, 65], for such fractional filling system, the ground state generally is the linear combination of Slater determinants. There is usually a serious sign problem for fractional filling. That means one can not naively use determinant quantum Monte-Carlo (DQMC) algorithm [87, 88] to model MATBCB. To realize

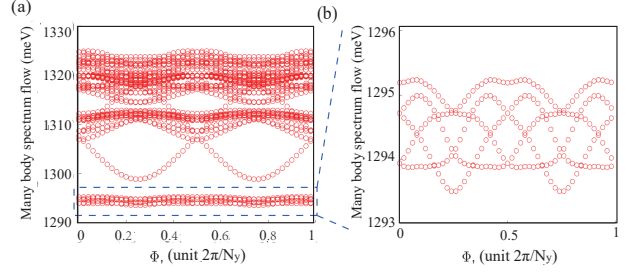


FIG. 6. (a) The spectrum flow under adiabatic flux insertion $k_y \rightarrow k_y + \Phi/N_y$ under chiral limit. (b) The zoomed in of low energy window in (a). One can examine that the states related by $G_1/2$ will keep almost two-fold degeneracy during flux inserting. The ten-fold quasi-degenerate ground states braid with each other as flux varying, while do not mix with higher energy states. These 10 states can be considered as the FCI topological ground state candidates. The gap between ground state manifold and higher energy states is about 5 – 12meV, While the width of ground state manifold is approximately 1 – 2meV.

the sign problem free simulation of Hamiltonian Eq. (11), like using exact diagonalization (ED), one needs to make use of symmetry to reduce the matrix block dimension, e.g. the particle number conservation. The particle number is defined by the filling factor $\nu = \frac{N_e}{N_x N_y}$. According to the vortexability formalism [70, 72], for $\nu = 1/5$, $C = 2$ system with contact interaction, it is expected to host a translation symmetry reserved FCI phase. So we will focus on $\nu = 1/5$ in this manuscript. In addition, one can use translation symmetry to consider smaller block, where each block or \mathbf{K} sector is labeled by total momentum [89]. Total momentum will be restricted in the first mBZ, i.e., $K_i \rightarrow \text{mod}(K_i, N_i)$, $i = x, y$.

Empirically, we expect relatively strong interaction would stabilize FCI phase. So we choose a relative large gate distance $d = 1000a \approx 36a_M$ and small dielectric constant $\epsilon_r = 1$ in following simulation. Here a is the monolayer lattice constant while a_M is the moiré superlattice constant.

Fig. 5 shows the many-body energy spectrum for $\nu = 1/5$ MATBCB system in the chiral limit with size 4×5 \mathbf{k} points. We will use the same parameters in the following simulation unless otherwise specified. It can be seen that there is a ten-fold quasi-degenerate ground state. The gap between ground state manifold and higher excitation states is about 10 – 12meV. The ground state at $K = 5, 6 \dots 9$ and $K = 15, 16 \dots 19$ sector can be approximately related by $G_1/2$ vector. Later we will show that additionally, the lowest ground state at different \mathbf{K} sector can also be related by $G_2/2$ from the spectrum flow under adiabatic flux inserting. One can conjecture that in putative topological degenerate ground state manifold, the ground state degeneracy(GSD) is 10. However, one should keep in mind that up to now we can not claim there is FCI phase in $\nu = 1/5$ MATBCB. We still have to inspect the ground state spectrum flow under adiabatic flux inserting [6, 90]. The ground states should keep in the low energy subspace without gap closing with other higher energy states, which means the GSD should be stable under

the adiabatic variation of boundary condition.

In Fig. 6, we show the corresponding spectrum flow for the same size and filling. We adapt the periodic boundary condition in k_y direction and let the momentum occur global shift $k_y \rightarrow k_y + \Phi/N_y$. It can be considered as one rolls k_y direction as a cylinder and inserts flux adiabatically along the cylinder axis. One can see the putative GSD=10 is stable in spectrum flow. The almost two-fold degeneracy for low energy state related by $G_1/2$ is preserved during flux inserting. When $\Phi \in [0, 2\pi/N_y)$, one can see that there is a non-trivial braiding between quasi-degenerate ground states. Moreover, in Fig. 6 one can observe that spectrum flow is symmetric about $\Phi_0 = \pi/N_y = \pi/5$. That means the lowest many-body spectrum is also invariant under the translation $G_2/2$. This indicates in many-body level, there may be similar folding rule along $\mathbf{Q} = (G_1/2, G_2/2)$ like single particle counterpart [70, 71]. In simulation, one should be cautious that keeping aspect ratio to be compatible is important. Otherwise the simulation may not approach 2d thermodynamic limit and spurious energy gap may emerge [6]. One can notice that when Φ changes from 0 to $2\pi/N_y$, N_y of k_y cuts exchange with each other. However their relative relationship in momentum space is unchanged. So $2\pi/N_y$ is one of the spectrum flow period.

In addition, one can also consider the many body Chern number [20, 91, 92] of the ten-fold degenerate states under chiral limit. By adiabatically inserting the flux along both direction of torus, one can get $C_{many} = \frac{1}{2\pi} \int_0^{2\pi} d\theta_x \int_0^{2\pi} d\theta_y F(\theta_x, \theta_y)$. It is also convenient to use the similar formalism like Eq. 10 in an effective discrete flux lattice. We get the total many body Chern number $|C_{tot}| = 4$. The many body Chern number $|C_{many}| = 2/5$ is the average of C_{tot} over ten-fold degenerate ground state, which is directly related to many body Hall conductivity. The many-body Chern number $|C_{many}|$ can be related to the Chern number of single particle band $|C_{single}|$ via $|C_{many}| = |C_{single}| \nu$ (ν is the filling fraction) [93], in consistence with former work in the Hofstadter model [94]. Since the C_{many} is a fractional one, it has ruled out some symmetry breaking Chern insulator phase like quantum anomalous Hall crystal [93].

Finally in this section, even if the spectrum flow shows that there could be topologically degenerate states in $\nu = 1/5$ MATBCB, one still can not distinguish FCI, potential commensurate charge density wave (CDW) and other competing phases [42]. To get the smoking gun evidence of FCI phase, one still has to diagnose the topological nature of many body ground state like many body entanglement. In the next section, we will settle down the FCI phase via particle entanglement spectrum (PES) and study the phase transition induced by chiral ratio variation through monitoring the PES gap.

V. THE PARTICLE ENTANGLEMENT SPECTRUM FOR MATBCB AND QUASI-HOLE COUNTING

To reveal the exotic quasi-hole excitation in putative FCI phase, one can consider the particle entanglement spectrum

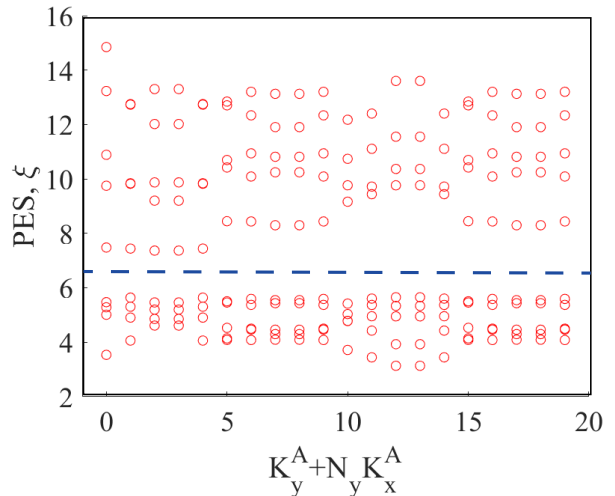


FIG. 7. The PES of ten-fold ground state density matrix for chiral limit $\kappa = w_{AA}/w_{AB} = 0$. The PES is labelled by the total momentum of subsystem A K^A . The spectrum almost gather at $\xi < 16$ regime, while other data with higher values can be considered as noise. There is an apparent PES gap at $\xi \approx 6.5$. One can extract the PES quasi-hole counting at each K^A (total momentum of subsystem A) sector under the PES gap. For $K^A = 0, 1 \dots 4$, there are 4 states per sector. While for $K^A = 5, 6 \dots 19$, there are 5 states per sector. The total number of quasi-hole is 95 (for 4×5 momentum space size). The counting obeys the $(1, 5)_{C=2}$ GPP based on Halperin spin singlet ansatz as argued in main text.

(PES) [95] for ground state or ground state manifold. The quasi-hole counting for FCI phase will obey generalized Pauli principle (GPP) and depend on the topology of base manifold [6, 32]. So the PES quasi-hole counting will be a smoking gun evidence of FCI phase and help one rule out CDW phase or other topologically trivial competing phases. Recently, PES has been widely used in FCI or FQAHE candidates from Moiré system [35, 96–98] and R5G system [26]. Briefly speaking, PES is the eigenvalue of the reduced density matrix which bipartites the system in particle number (Fock) space. The mostly used reduced density matrix is to trace over the all possible half of the particle configurations in subsystem B in the model and keep the other half subsystem A [95]. However, the particle number of subsystem A and B are not necessarily to be the same.

Following Ref. [99], one can consider the pure state PES for simplicity. The ground state of fractional filling MATBCB generally is a linear combination of Slater determinants. If the ground state is non-degenerate, one can write down the

ground state as follow, (which is a pure state):

$$\begin{aligned}
|\psi_0\rangle &= \begin{pmatrix} a_1 \\ a_2 \\ \dots \\ a_n \end{pmatrix} = a_1 \begin{pmatrix} 1 \\ 0 \\ \dots \\ 0 \end{pmatrix} + \dots + a_n \begin{pmatrix} 0 \\ 0 \\ \dots \\ 1 \end{pmatrix} = a_1 \phi_1 + \dots + a_n \phi_n \\
&= \frac{1}{\sqrt{C(N_e, N_A)}} [a_1 (\sum_{A,B} (-1)^{\text{sign}_1(A,B)} \phi_1^A \phi_1^B) + \dots + \\
&a_n (\sum_{A,B} (-1)^{\text{sign}_n(A,B)} \phi_n^A \phi_n^B)].
\end{aligned} \tag{14}$$

Here ϕ_1, \dots, ϕ_n are Slater determinants in the first quantization form. By using the famous Laplace decomposition formalism for determinant in linear algebra, one can expand each Slater determinant with A and B sub-determinants, the sign like $\text{sign}_1(A, B)$ is determined by the sign of the algebraic cofactor. $\frac{1}{\sqrt{C(N_e, N_A)}} = \frac{1}{\sqrt{(N_e!)/[(N_A)!(N_B)!]}}$ occurred in prefactor is for normalization. In principle one can write out the bipartition of wave function $|\psi_0\rangle$ under the particle conserved basis with particle number $N_A = N_e/2$. Its dimension is $C(N, N_A) = N!/[N_A!(N - N_A)!]$. Here $N = N_x N_y$ is the number of total orbital. The nonzero singular values of matrix $|\psi_0\rangle_{C(N, N_A) \times C(N, N_B)}$ are denoted as $\{\exp(-\xi_i/2)\}$, where $\{\xi_i\}$ is the PES.

However, the above procedure only applies to the pure state or non-degenerate state. The situation for mixed state or degenerate state in our $\nu = 1/5$ MATBCB system will be more complicated. One has to consider the following mixed state density matrix consisting of degenerate states [6, 26].

$$\rho = \frac{1}{D} \sum_{i=1}^D |\psi_i\rangle \langle \psi_i|. \tag{15}$$

Generally speaking, each term in Eq. (15) will not share common A, B bipartitions. However, one can still find a large enough subspace (such as the $C(N, N_A) \times C(N, N_B)$ dimension space mentioned above.) to trace over the all possible B part term by term in Eq. 15, which means one can always do the SVD term by term and then get the reduced density matrix ρ_A . The eigenvalues of ρ_A will be $\{\exp(-\xi_i)\}$ which is related to PES $\{\xi_i\}$.

$$\begin{aligned}
|\psi_i\rangle &= U_i S_i V_i^\dagger, \\
\rho_A &= Tr_B[\rho] = \frac{1}{D} \sum_{i=1}^D Tr_B[|\psi_i\rangle \langle \psi_i|] = \frac{1}{D} \sum_{i=1}^D U_i S_i^2 U_i^\dagger.
\end{aligned} \tag{16}$$

After introducing the algorithm of PES, in order to physically interpret the result of PES, we now briefly review the generalized Pauli principle (GPP) and its higher Chern number generalization [6, 32]. For the simplest $C = 1$ case, one has $(k, r)_{C=1}$ GPP in $\nu = k/r$ FCI phase for its quasi-hole counting. Concretely, in Fock space, there should be no more than k occupied states among arbitrary consecutive r orbitals. For FCI phase, the number of quasi-hole state under PES gap should be consistent with the configuration number predicted by GPP. The quasi-hole counting in GPP will be sensitive to the

base manifold topology. For example, on sphere the orbitals align in a chain. However for our case on T^2 (torus), the orbitals align in a ring which means the occupation at the end should also obey the $(k, r)_{C=1}$ constraint. For $\nu = 1/3$, there is an analytical solution for $(1, 3)_{C=1}$ GPP configuration number $N_x N_y \frac{(N_x N_y - 2N_A - 1)!}{(N_x N_y - 3N_A)!(N_A)!}$ [6], which corresponds to Laughlin state quasi-hole counting. Unfortunately, for the case of general $(k, r)_{C=1}$, the GPP quasi-hole counting is related to so called Jack polynomial [100, 101], for which there is no simple form in general. On the other hand, numerically one can always enumerate all configurations obeying $(k, r)_{C=1}$ GPP on torus for not so large size system. For higher Chern number $C > 1$ situation, it is believed that the quasi-particle will carry an additional internal SU(C) degree of freedom, which bring more constraints. This SU(C) symmetry is usually called color symmetry like high energy community. Specially, when $C = 2$, the SU(2) symmetry can be considered as an effective (pseudo) spin degree of freedom. During bipartition, it is reasonable to assume that the internal SU(C) symmetry is preserved in each subsystem A and B. That means in subsystem A the quasi-particle should form (Halperin) color singlet or minimize the net color polarization [32]. For the particle with the same color, they will obey the $(k, r)_{C=1}$ GPP. While for the counterpart with different color they will not have such constraint except the hard core condition. That means two particles can not occupy the same orbital even if they have different color. An interpretable analogy for $C = 2$ case is the spinful Pauli exclusive principle under strong intra orbital interaction limit in atomic physics. The particle with different spin will not occupy the same orbital.

From the above analysis, now one can come back and inspect the PES of $\nu = 1/5$ MATBCB. In Fig. 7, we show the PES of the density matrix consists of 10 fold topological ground state candidates. There is an apparent PES gap at about $\xi = 6.5$ as shown by the blue dashed line. One can check that there are 4 quasi-hole states under PES gap in each $K^A = 0, 1 \dots 4$ sector while 5 low quasi-hole states in each $K^A = 5, 6 \dots 19$ sector. The total number of quasi-hole state is 95 for $N_x = 4, N_y = 5, N_A = 2$. Such quasi-hole counting is coincident with $(1, 5)_{C=2}$ GPP. One can interpret this result as follows. In our case, $N_x = 4, N_y = 5, N_e = 4, N_A = 2$. One can enumerate the Halperin spin singlet in subsystem A. The possibility to get spin up or down particle are the same $1/2$ ($1/C$). So the number of configurations which obeys $(1, 5)_{C=2}$ GPP is $\frac{20 \times 19}{2} = 95$. While for CDW phase, the quasi-hole counting is significantly different, which is given by $n = dC(N_e, N_A)$ [42, 102]. d is the number of CDW order. Up to now, one can claim that $\nu = 1/5$ MATBCB under chiral limit hosts $C = 2$ abelian FCI phase. MATBCB can naturally realize the $C = 2$ FCI without stacking $C = 1$ FCI. For the later one, it is hard to guarantee the position of the valley is invariant when stacking.

On the other hand, it is important to check if such $C = 2$ FCI is robust when it deviates from the ideal condition [103]. For example, the influence of chiral ratio $\kappa = w_{AA}/w_{AB}$ [66–68]. When $\kappa \neq 0$, the lowest single particle bands will be broadened. The kinetic term will compete with projective interaction. And quasi-particle will generally feel a non-

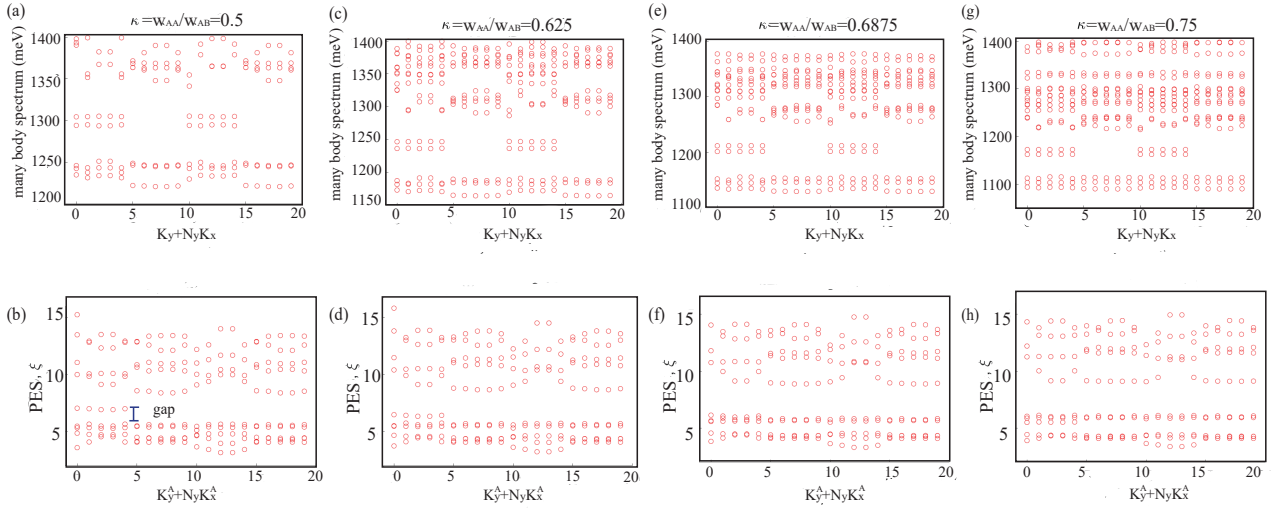


FIG. 8. (a) The many-body energy spectrum of MATBCB for $\kappa = w_{AA}/w_{AB} = 0.5$. One can see that the original ten-fold ground states get closer to higher energy states. (b) The PES of 10 fold degenerate ground state density matrix for the same κ . The PES gap is illustrated by the blue line segment. The location of PES gap is the same in (d), (f), and (h). The quasi-hole counting under PES gap is the same as $\kappa = 0$ case, which indicates FCI phase is stable under the variation of chiral ratio to some extent. There are five states above the PES gap which locate at $\xi \approx 7$ and $K^A = 0, 1 \dots 4$. Compared with $\kappa = 0$ case, they are approaching the original quasi-hole manifold when κ increases to 0.5. So we expect when κ increases to a critical value, these five higher states will meet the lower quasi-hole states. (c) The many-body energy spectrum of MATBCB for $\kappa = 0.625$. (d) The PES for $\kappa = 0.625$. The five states mentioned above get very close to lower quasi-hole states. (e) The many-body energy spectrum of MATBCB for $\kappa = 0.6875$. (f) The PES for $\kappa = 0.6875$. The five states mentioned above have partially collapsed to lower quasi-hole states. (g) The many-body energy spectrum of MATBCB for $\kappa = 0.75$. (h) The PES for $\kappa = 0.75$. The five states mentioned above have completely collapsed to lower quasi-hole states. This may be interpreted as the violation of the hard core condition. After phase transition, the particle with different pseudo spin can occupy the same orbital. So the number of lower quasi-hole states increase extra $\frac{20}{2^2} = 5$.

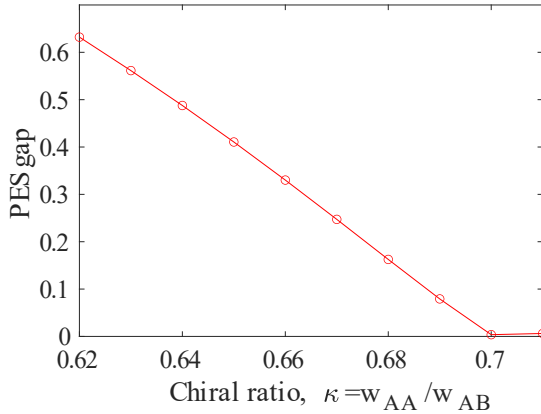


FIG. 9. The PES gap versus chiral ratio. The PES gap is defined as $|\min(\xi(n = 5, K^A = 0 \dots 4)) - \max(\xi(n = 4, K^A = 0 \dots 4), \xi(n = 5, K^A = 5 \dots 19))|$. The gap decreases with increasing chiral ratio and becomes close to zero at $\kappa_c \approx 0.7050$, suggesting a phase transition.

uniform Berry curvature. One can expect there is a critical chiral ratio where the FCI phase breaks down and phase transition happens. We will locate such phase transition according to PES gap [6]. In Fig. 8, we show the many-body energy spectrum and the PES of 10 fold degenerate mixed

state under different chiral ratio $\kappa = 0.5, 0.625, 0.6875, 0.75$ while keeping other parameters unchanged. When κ increases, there are 5 states approaching the original quasi-hole manifold at $\kappa = 0$. As κ reaches the critical value κ_c , these 5 states will collapse on lower quasi-hole manifold. Denoting $|\min(\xi(n = 5, K^A = 0 \dots 4)) - \max(\xi(n = 4, K^A = 0 \dots 4), \xi(n = 5, K^A = 5 \dots 19))|$ as the PES gap, the PES gap closing phase transition can be interpreted as the violation of hard core condition. That means after phase transition, the particle with different pseudo spin can occupy the same orbital. So one has additional $\frac{20}{2^2} = 5$ configurations. It is not difficult to understand this since when κ increases, the kinetic term can be comparable with interaction at a critical value. By keeping track of the PES gap evolution about chiral ratio κ , we find that the PES gap decreases as κ increases, shown in Fig. 9. And there is a PES gap closing at $\kappa_c \approx 0.7050$, which indicates a phase transition.

To summarize this section, we have obtained the smoking gun evidence of the existence of $C = 2$ FCI phase in $\nu = 1/5, \kappa = 0$ MATBCB via PES quasi-hole counting. The number of quasi-hole states under PES gap obeys $(1, 5)_{C=2}$ GPP. As chiral ratio κ increases, there will be PES gap closing at $\kappa_c \approx 0.7050$. The quasi-hole counting will change, which indicates the violation of the hard core condition. However, recall that in section IV we get the spectrum flow with about $5 - 12$ meV gap between ground state manifold and higher

energy states. This gap is not large enough compared with the ground state manifold width $\approx 1.5\text{meV}$. One may expect a weak external magnetic field or exchange interaction [104] is still needed to stabilize the FCI phase [13, 94, 105, 106], which will be left for future work.

VI. CONCLUSION AND DISCUSSION

In this manuscript, we study a putative $C = 2$ abelian FCI phase in $\nu = 1/5, \kappa = 0$ MATBCB. In the single particle level, we obtain the lowest topological flat bands with $C = \pm 2$. The band width is about $1.5 \times 10^{-3}\text{meV}$ at the first magic angle $\phi = 1.608^\circ$. The almost uniform Berry curvature and tiny trace condition violation indicate the ideal quantum geometry condition to host FCI phase. In the many-body level, we first present the many body energy spectrum and spectrum flow for projected Coulomb interaction model of MATBCB. We find there is topological ground state manifold candidate with $\text{GSD}=10$. Next we examine the PES quasi-hole counting of the ground state manifold candidate. We find the counting meets the $(1, 5)_{C=2}$ GPP as Halperin spin singlet. This counting is a smoking gun evidence of $C = 2$ FCI. When the parameters are not ideal, such as the chiral ratio deviates from zero, there will be a phase transition which breaks the FCI phase. We estimate that $\kappa_c \approx 0.7050$. More comprehensive research on the FCI relevant phase transition will be left for future work.

However, one should still keep in mind that the results and arguments above are all built on the assumption that the translation symmetry is preserved. When the translation symmetry is broken, the internal $\text{SU}(C)$ color symmetry can be entangled with spatial symmetry. Especially, the $\text{SU}(C)$ symmetry and spatial translation symmetry will combine to form a generalized (pseudo) magnetic translation symmetry [33, 107]. In that case, we conjecture that the $\text{SU}(C)$ color symmetry will also be broken accompanied with the translation symmetry broken. An example is the $\nu = 1/6, C = 2$ flat band system [70]. At that situation, Halperin color singlet quasi-hole counting ansatz based $(k, r)_C$ GPP may be violated. A more general pseudo potential method under $n_x - k_y$ basis has to be used [8, 33, 108]. Moreover, under $n_x - k_y$ basis it is convenient to simulate fractional filling system with numerical methods like DMRG [66, 67], which

can handle larger size compared with ED. Compared with analytical pseudopotential method, it can model the situation beyond thin cylinder limit [33]. It is also very interesting and valuable to search for possible non-abelian FCI phase in TBCB system. The problem about the coexistence of FCI phase and charge ordered phase [92] is also beyond one's intuitive knowledge, which may occur in TBCB. Also, it is worth to find the connection between higher Chern number FCI and topological quantum chemistry in order to find material realization [109]. For spinful case there may be much richer competing phases, e.g., ferromagnetic phase. Also it is very interesting to study the spin-valley locking effect and the competition between FCI and valley-polarized phase like MoTe_2 [14] or spin-valley composite phase in moiré trilayer graphene [110, 111] case. The open questions mentioned above are worth further research in the future.

ACKNOWLEDGEMENTS

We thank Jian Kang, Wei Li, Daniel E.Parker, Han-Qing Wu, Jie Wang, Ying-Hai Wu, Jia-Qi Cai, Gao-Pei Pan, Ming-Rui Li, Jun-Kai Dong, Ti-Xuan Tan, Zhongqing Guo, Wang-Qian Miao, Yunzhe Liu, Xiaohan Wan, Mu-Wei Wu for valuable discussions. J. Z. M. and D. X. Y. are supported by National Key Research and Development Program of China (2022YFA1402802), National Natural Science Foundation of China (92165204), Leading Talent Program of Guangdong Special Projects (201626003), Guangdong Provincial Key Laboratory of Magnetoelectric Physics and Devices (Grant No. 656 2022B1212010008), Guangdong Fundamental Research Center for Magnetoelectric Physics, and Shenzhen International Quantum Academy. J.-Y. C. is supported by National Natural Science Foundation of China (12304186), Open Research Fund Program of the State Key Laboratory of Low-Dimensional Quantum Physics (KF202207), Fundamental Research Funds for the Central Universities, Sun Yat-sen University (23qnp60), Innovation Program for Quantum Science and Technology 2021ZD0302100, Guangzhou Basic and Applied Basic Research Foundation (2024A04J4264), the Guangdong Basic and Applied Basic Research Foundation (2024A1515013065). R.Z.H is supported by a postdoctoral fellowship from the Special Research Fund (BOF) of Ghent University.

-
- [1] S. Das Sarma, M. Freedman, and C. Nayak, Topologically protected qubits from a possible non-abelian fractional quantum hall state, *Phys. Rev. Lett.* **94**, 166802 (2005).
- [2] C. Nayak, S. H. Simon, A. Stern, M. Freedman, and S. Das Sarma, Non-abelian anyons and topological quantum computation, *Rev. Mod. Phys.* **80**, 1083 (2008).
- [3] E. Tang, J.-W. Mei, and X.-G. Wen, High-temperature fractional quantum hall states, *Phys. Rev. Lett.* **106**, 236802 (2011).
- [4] T. Neupert, L. Santos, C. Chamon, and C. Mudry, Fractional quantum hall states at zero magnetic field, *Phys. Rev. Lett.* **106**, 236804 (2011).
- [5] K. Sun, Z. Gu, H. Katsura, and S. Das Sarma, Nearly flatbands with nontrivial topology, *Phys. Rev. Lett.* **106**, 236803 (2011).
- [6] N. Regnault and B. A. Bernevig, Fractional chern insulator, *Phys. Rev. X* **1**, 021014 (2011).
- [7] D. N. Sheng, Z.-C. Gu, K. Sun, and L. Sheng, Fractional quantum hall effect in the absence of landau levels, *Nature Communications* **2**, 389 (2011).
- [8] X.-L. Qi, Generic wave-function description of fractional quantum anomalous hall states and fractional topological insulators, *Phys. Rev. Lett.* **107**, 126803 (2011).

- [9] H. Park, J. Cai, E. Anderson, Y. Zhang, J. Zhu, X. Liu, C. Wang, W. Holtzmann, C. Hu, Z. Liu, T. Taniguchi, K. Watanabe, J.-H. Chu, T. Cao, L. Fu, W. Yao, C.-Z. Chang, D. Cobden, D. Xiao, and X. Xu, Observation of fractionally quantized anomalous hall effect, *Nature* **622**, 74 (2023).
- [10] J. Cai, E. Anderson, C. Wang, X. Zhang, X. Liu, W. Holtzmann, Y. Zhang, F. Fan, T. Taniguchi, K. Watanabe, Y. Ran, T. Cao, L. Fu, D. Xiao, W. Yao, and X. Xu, Signatures of fractional quantum anomalous hall states in twisted mote₂, *Nature* **622**, 63 (2023).
- [11] F. Xu, Z. Sun, T. Jia, C. Liu, C. Xu, C. Li, Y. Gu, K. Watanabe, T. Taniguchi, B. Tong, J. Jia, Z. Shi, S. Jiang, Y. Zhang, X. Liu, and T. Li, Observation of integer and fractional quantum anomalous hall effects in twisted bilayer mote₂, *Phys. Rev. X* **13**, 031037 (2023).
- [12] Z. Lu, T. Han, Y. Yao, A. P. Reddy, J. Yang, J. Seo, K. Watanabe, T. Taniguchi, L. Fu, and L. Ju, Fractional quantum anomalous hall effect in multilayer graphene, *Nature* **626**, 759 (2024).
- [13] Y. Xie, A. T. Pierce, J. M. Park, D. E. Parker, E. Khalaf, P. Ledwith, Y. Cao, S. H. Lee, S. Chen, P. R. Forrester, K. Watanabe, T. Taniguchi, A. Vishwanath, P. Jarillo-Herrero, and A. Yacoby, Fractional chern insulators in magic-angle twisted bilayer graphene, *Nature* **600**, 439 (2021).
- [14] C. Wang, X.-W. Zhang, X. Liu, Y. He, X. Xu, Y. Ran, T. Cao, and D. Xiao, Fractional chern insulator in twisted bilayer mote₂, *Phys. Rev. Lett.* **132**, 036501 (2024).
- [15] N. Mao, C. Xu, J. Li, T. Bao, P. Liu, Y. Xu, C. Felser, L. Fu, and Y. Zhang, Lattice relaxation, electronic structure and continuum model for twisted bilayer mote₂ (2023), arXiv:2311.07533 [cond-mat.str-el].
- [16] Y. Jia, J. Yu, J. Liu, J. Herzog-Arbeitman, Z. Qi, N. Regnault, H. Weng, B. A. Bernevig, and Q. Wu, Moiré fractional chern insulators i: First-principles calculations and continuum models of twisted bilayer mote₂ (2023), arXiv:2311.04958 [cond-mat.mes-hall].
- [17] J. Yu, J. Herzog-Arbeitman, M. Wang, O. Vafek, B. A. Bernevig, and N. Regnault, Fractional chern insulators vs. non-magnetic states in twisted bilayer mote₂ (2023), arXiv:2309.14429 [cond-mat.mes-hall].
- [18] W. Yang, D. Zhai, F.-R. Fan, and W. Yao, Fractional quantum anomalous hall effect in a semimetal (2024), arXiv:2405.01829 [cond-mat.mes-hall].
- [19] V. Crépel, N. Regnault, and R. Queiroz, Chiral limit and origin of topological flat bands in twisted transition metal dichalcogenide homobilayers, *Communications Physics* **7**, 146 (2024).
- [20] F. Chen, W.-W. Luo, W. Zhu, and D. N. Sheng, Robust non-abelian even-denominator fractional chern insulator in twisted bilayer mote₂ (2024), arXiv:2405.08386 [cond-mat.str-el].
- [21] P. Sharma, Y. Peng, and D. N. Sheng, Topological quantum phase transitions driven by displacement fields in the twisted mote₂ bilayers (2024), arXiv:2405.08181 [cond-mat.mes-hall].
- [22] B. Li and F. Wu, Variational mapping of chern bands to landau levels: Application to fractional chern insulators in twisted mote₂ (2024), arXiv:2405.20307 [cond-mat.mes-hall].
- [23] T. Lu and L. H. Santos, Fractional chern insulators in twisted bilayer mote₂: A composite fermion perspective (2024), arXiv:2406.03530 [cond-mat.str-el].
- [24] Z. Dong, A. S. Patri, and T. Senthil, Stability of anomalous hall crystals in multilayer rhombohedral graphene (2024), arXiv:2403.07873 [cond-mat.str-el].
- [25] Z. Guo, X. Lu, B. Xie, and J. Liu, Theory of fractional chern insulator states in pentalayer graphene moiré superlattice (2023), arXiv:2311.14368 [cond-mat.str-el].
- [26] Z. Dong, A. S. Patri, and T. Senthil, Theory of fractional quantum anomalous hall phases in pentalayer rhombohedral graphene moiré structures (2023), arXiv:2311.03445 [cond-mat.str-el].
- [27] T. Tan and T. Devakul, Parent berry curvature and the ideal anomalous hall crystal (2024), arXiv:2403.04196 [cond-mat.mes-hall].
- [28] J. Dong, T. Wang, T. Wang, T. Soejima, M. P. Zaletel, A. Vishwanath, and D. E. Parker, Anomalous hall crystals in rhombohedral multilayer graphene i: Interaction-driven chern bands and fractional quantum hall states at zero magnetic field (2023), arXiv:2311.05568 [cond-mat.str-el].
- [29] B. Zhou, H. Yang, and Y.-H. Zhang, Fractional quantum anomalous hall effects in rhombohedral multilayer graphene in the moiréless limit and in coulomb imprinted superlattice (2023), arXiv:2311.04217 [cond-mat.str-el].
- [30] J. Herzog-Arbeitman, Y. Wang, J. Liu, P. M. Tam, Z. Qi, Y. Jia, D. K. Efetov, O. Vafek, N. Regnault, H. Weng, Q. Wu, B. A. Bernevig, and J. Yu, Moiré fractional chern insulators ii: First-principles calculations and continuum models of rhombohedral graphene superlattices (2023), arXiv:2311.12920 [cond-mat.mes-hall].
- [31] J. Dong, J. Wang, P. J. Ledwith, A. Vishwanath, and D. E. Parker, Composite fermi liquid at zero magnetic field in twisted mote₂, *Phys. Rev. Lett.* **131**, 136502 (2023).
- [32] A. Sterdyniak, C. Repellin, B. A. Bernevig, and N. Regnault, Series of abelian and non-abelian states in $c > 1$ fractional chern insulators, *Phys. Rev. B* **87**, 205137 (2013).
- [33] Y.-L. Wu, N. Regnault, and B. A. Bernevig, Haldane statistics for fractional chern insulators with an arbitrary chern number, *Phys. Rev. B* **89**, 155113 (2014).
- [34] Z. Liu, E. J. Bergholtz, H. Fan, and A. M. Läuchli, Fractional chern insulators in topological flat bands with higher chern number, *Phys. Rev. Lett.* **109**, 186805 (2012).
- [35] J. Wang and Z. Liu, Hierarchy of ideal flatbands in chiral twisted multilayer graphene models, *Phys. Rev. Lett.* **128**, 176403 (2022).
- [36] Y.-F. Wang, H. Yao, C.-D. Gong, and D. N. Sheng, Fractional quantum hall effect in topological flat bands with chern number two, *Phys. Rev. B* **86**, 201101(R) (2012).
- [37] J. Xie, Z. Huo, X. Lu, Z. Feng, Z. Zhang, W. Wang, Q. Yang, K. Watanabe, T. Taniguchi, K. Liu, Z. Song, X. C. Xie, J. Liu, and X. Lu, Even- and odd-denominator fractional quantum anomalous hall effect in graphene moire superlattices (2024), arXiv:2405.16944 [cond-mat.mes-hall].
- [38] C. Wang, X.-W. Zhang, X. Liu, J. Wang, T. Cao, and D. Xiao, Higher landau-level analogues and signatures of non-abelian states in twisted bilayer mote₂ (2024), arXiv:2404.05697 [cond-mat.str-el].
- [39] L. Zhang and X.-Y. Song, Moore-read state in half-filled moiré chern band from three-body pseudo-potential (2024), arXiv:2403.11478 [cond-mat.str-el].
- [40] C. Xu, N. Mao, T. Zeng, and Y. Zhang, Multiple chern bands in twisted mote₂; and possible non-abelian states (2024), arXiv:2403.17003 [cond-mat.str-el].
- [41] A. P. Reddy, N. Paul, A. Abouelkomsan, and L. Fu, Non-abelian fractionalization in topological minibands (2024), arXiv:2403.00059 [cond-mat.mes-hall].
- [42] H. Liu, Z. Liu, and E. J. Bergholtz, Non-abelian fractional chern insulators and competing states in flat moiré bands (2024), arXiv:2405.08887 [cond-mat.str-el].

- [43] Z. Liu, B. Mera, M. Fujimoto, T. Ozawa, and J. Wang, Theory of generalized landau levels and implication for non-abelian states (2024), arXiv:2405.14479 [cond-mat.mes-hall].
- [44] A.-L. He, W.-W. Luo, H. Yao, and Y.-F. Wang, Non-abelian fractional chern insulator in disk geometry, *Phys. Rev. B* **101**, 165127 (2020).
- [45] R. Kobayashi, Y. Zhang, N. Manjunath, and M. Barkeshli, Crystalline invariants of fractional chern insulators (2024), arXiv:2405.17431 [cond-mat.str-el].
- [46] H. Liu, R. Perea-Causin, and E. J. Bergholtz, Parafermions in moiré minibands (2024), arXiv:2406.08546 [cond-mat.str-el].
- [47] H. Park, J. Cai, E. Anderson, X.-W. Zhang, X. Liu, W. Holtzmann, W. Li, C. Wang, C. Hu, Y. Zhao, T. Taniguchi, K. Watanabe, J. Yang, D. Cobden, J.-H. Chu, N. Regnault, B. A. Bernevig, L. Fu, T. Cao, D. Xiao, and X. Xu, Ferromagnetism and topology of the higher flat band in a fractional chern insulator (2024), arXiv:2406.09591 [cond-mat.mes-hall].
- [48] F. Xu, X. Chang, J. Xiao, Y. Zhang, F. Liu, Z. Sun, N. Mao, N. Peshcherenko, J. Li, K. Watanabe, T. Taniguchi, B. Tong, L. Lu, J. Jia, D. Qian, Z. Shi, Y. Zhang, X. Liu, S. Jiang, and T. Li, Interplay between topology and correlations in the second moiré band of twisted bilayer mote2 (2024), arXiv:2406.09687 [cond-mat.mes-hall].
- [49] M.-R. Li, A.-L. He, and H. Yao, Magic-angle twisted bilayer systems with quadratic band touching: Exactly flat bands with high chern number, *Phys. Rev. Res.* **4**, 043151 (2022).
- [50] Y. Zhao and X.-F. Shi, The fractional chern insulator with rydberg-dressed neutral atoms (2022), arXiv:2206.04213 [cond-mat.quant-gas].
- [51] A. González-Tudela and J. I. Cirac, Cold atoms in twisted-bilayer optical potentials, *Phys. Rev. A* **100**, 053604 (2019).
- [52] X.-T. Wan, C. Gao, and Z.-Y. Shi, Fractal spectrum in twisted bilayer optical lattice (2024), arXiv:2404.08211 [cond-mat.mes-hall].
- [53] C. Zhang, Z. Fan, B. Capogrosso-Sansone, and Y. Deng, Dipolar bosons in a twisted bilayer geometry (2024), arXiv:2405.16425 [cond-mat.quant-gas].
- [54] J.-H. Zeng, Q. Zhu, and L. He, Dynamical moiré systems in twisted bilayer optical lattices (2024), arXiv:2405.20732 [cond-mat.quant-gas].
- [55] C. Wang, F.-M. Liu, M.-C. Chen, H. Chen, X.-H. Zhao, C. Ying, Z.-X. Shang, J.-W. Wang, Y.-H. Huo, C.-Z. Peng, X. Zhu, C.-Y. Lu, and J.-W. Pan, Realization of fractional quantum hall state with interacting photons, *Science* **384**, 579 (2024), <https://www.science.org/doi/pdf/10.1126/science.ado3912>.
- [56] S. Sarkar, X. Wan, S.-Z. Lin, and K. Sun, Symmetry-based classification of exact flat bands in single and bilayer moiré systems (2023), arXiv:2310.02218 [cond-mat.mes-hall].
- [57] J. Herzog-Arbeitman, A. Chew, and B. A. Bernevig, Magnetic bloch theorem and reentrant flat bands in twisted bilayer graphene at 2π flux, *Phys. Rev. B* **106**, 085140 (2022).
- [58] Y. Soeda, K. Asaga, and T. Fukui, Moiré landau levels of a C_4 -symmetric twisted bilayer system in the absence of a magnetic field, *Phys. Rev. B* **105**, 165422 (2022).
- [59] C. Madroño, G. A. D. Castro, and R. Paredes, Localized and extended phases in square moiré patterns (2024), arXiv:2405.00811 [cond-mat.mes-hall].
- [60] P. M. Eugenio, Z.-X. Luo, A. Vishwanath, and P. A. Volkov, Tunable $t - t' - u$ hubbard models in twisted square homobilayers (2024), arXiv:2406.02448 [cond-mat.str-el].
- [61] P. M. Eugenio and O. Vafek, Twisted-bilayer fese and the fe-based superlattices, *SciPost Phys.* **15**, 081 (2023).
- [62] X. Wan, S. Sarkar, S.-Z. Lin, and K. Sun, Topological exact flat bands in two-dimensional materials under periodic strain, *Phys. Rev. Lett.* **130**, 216401 (2023).
- [63] Q. Xu, N. Tancogne-Dejean, E. V. Boström, D. M. Kennes, M. Claassen, A. Rubio, and L. Xian, Engineering 2d square lattice hubbard models in 90° twisted ge/snx ($x=s$, se) moiré superlattices (2024), arXiv:2406.05626 [cond-mat.str-el].
- [64] Z.-D. Song, B. Lian, N. Regnault, and B. A. Bernevig, Twisted bilayer graphene. ii. stable symmetry anomaly, *Phys. Rev. B* **103**, 205412 (2021).
- [65] B. Lian, Z.-D. Song, N. Regnault, D. K. Efetov, A. Yazdani, and B. A. Bernevig, Twisted bilayer graphene. iv. exact insulator ground states and phase diagram, *Phys. Rev. B* **103**, 205414 (2021).
- [66] J. Kang and O. Vafek, Non-abelian dirac node braiding and near-degeneracy of correlated phases at odd integer filling in magic-angle twisted bilayer graphene, *Phys. Rev. B* **102**, 035161 (2020).
- [67] T. Soejima, D. E. Parker, N. Bultinck, J. Hauschild, and M. P. Zaletel, Efficient simulation of moiré materials using the density matrix renormalization group, *Phys. Rev. B* **102**, 205111 (2020).
- [68] D. Parker, P. Ledwith, E. Khalaf, T. Soejima, J. Hauschild, Y. Xie, A. Pierce, M. P. Zaletel, A. Yacoby, and A. Vishwanath, Field-tuned and zero-field fractional chern insulators in magic angle graphene (2021), arXiv:2112.13837 [cond-mat.str-el].
- [69] J. Wang, S. Klevtsov, and Z. Liu, Origin of model fractional chern insulators in all topological ideal flatbands: Explicit color-entangled wave function and exact density algebra, *Phys. Rev. Res.* **5**, 023167 (2023).
- [70] J. Dong, P. J. Ledwith, E. Khalaf, J. Y. Lee, and A. Vishwanath, Many-body ground states from decomposition of ideal higher chern bands: Applications to chirally twisted graphene multilayers, *Phys. Rev. Res.* **5**, 023166 (2023).
- [71] P. J. Ledwith, A. Vishwanath, and E. Khalaf, Family of ideal chern flatbands with arbitrary chern number in chiral twisted graphene multilayers, *Phys. Rev. Lett.* **128**, 176404 (2022).
- [72] P. J. Ledwith, A. Vishwanath, and D. E. Parker, Vortexability: A unifying criterion for ideal fractional chern insulators (2022), arXiv:2209.15023 [cond-mat.str-el].
- [73] M. Fujimoto, D. E. Parker, J. Dong, E. Khalaf, A. Vishwanath, and P. Ledwith, Higher vortexability: zero field realization of higher landau levels (2024), arXiv:2403.00856 [cond-mat.mes-hall].
- [74] T. Fukui, Y. Hatsugai, and H. Suzuki, Chern numbers in discretized brillouin zone: Efficient method of computing (spin) hall conductances, *Journal of the Physical Society of Japan* **74**, 1674 (2005).
- [75] J. Herzog-Arbeitman, J. Yu, D. Călugăru, H. Hu, N. Regnault, C. Liu, S. D. Sarma, O. Vafek, P. Coleman, A. Tsvelik, Z. da Song, and B. A. Bernevig, Topological heavy fermion principle for flat (narrow) bands with concentrated quantum geometry (2024), arXiv:2404.07253 [cond-mat.str-el].
- [76] O. E. Sommer, X. Wen, and A. Vishwanath, Higher berry curvature from the wave function i: Schmidt decomposition and matrix product states (2024), arXiv:2405.05316 [cond-mat.str-el].
- [77] O. E. Sommer, A. Vishwanath, and X. Wen, Higher berry curvature from the wave function ii: Locally parameterized states beyond one dimension (2024), arXiv:2405.05323 [cond-mat.str-el].
- [78] S. Ohyama and S. Ryu, Higher berry phase from projected entangled pair states in (2+1) dimensions (2024),

- arXiv:2405.05325 [cond-mat.str-el].
- [79] J. Wang, J. Cano, A. J. Millis, Z. Liu, and B. Yang, Exact Landau level description of geometry and interaction in a flatband, *Phys. Rev. Lett.* **127**, 246403 (2021).
- [80] B. A. Bernevig, Z.-D. Song, N. Regnault, and B. Lian, Twisted bilayer graphene. i. matrix elements, approximations, perturbation theory, and a $k \cdot p$ two-band model, *Phys. Rev. B* **103**, 205411 (2021).
- [81] B. A. Bernevig, Z.-D. Song, N. Regnault, and B. Lian, Twisted bilayer graphene. iii. interacting hamiltonian and exact symmetries, *Phys. Rev. B* **103**, 205413 (2021).
- [82] B. A. Bernevig, B. Lian, A. Cowsik, F. Xie, N. Regnault, and Z.-D. Song, Twisted bilayer graphene. v. exact analytic many-body excitations in coulomb hamiltonians: Charge gap, goldstone modes, and absence of cooper pairing, *Phys. Rev. B* **103**, 205415 (2021).
- [83] F. Xie, A. Cowsik, Z.-D. Song, B. Lian, B. A. Bernevig, and N. Regnault, Twisted bilayer graphene. vi. an exact diagonalization study at nonzero integer filling, *Phys. Rev. B* **103**, 205416 (2021).
- [84] O. Vafek and J. Kang, Renormalization group study of hidden symmetry in twisted bilayer graphene with coulomb interactions, *Phys. Rev. Lett.* **125**, 257602 (2020).
- [85] R. N. C. Pfeifer, G. Evenbly, S. Singh, and G. Vidal, Ncon: A tensor network contractor for matlab (2015), arXiv:1402.0939 [physics.comp-ph].
- [86] F. Xie, Y. Fang, L. Chen, J. Cano, and Q. Si, Chern bands' optimally localized wannier functions and fractional chern insulators (2024), arXiv:2407.08920 [cond-mat.mes-hall].
- [87] G. Pan and Z. Y. Meng, The sign problem in quantum monte carlo simulations, in *Encyclopedia of Condensed Matter Physics (Second Edition)*, edited by T. Chakraborty (Academic Press, Oxford, 2024) second edition ed., pp. 879–893.
- [88] X. Zhang, G. Pan, X. Y. Xu, and Z. Y. Meng, Fermion sign bounds theory in quantum monte carlo simulation, *Phys. Rev. B* **106**, 035121 (2022).
- [89] A. W. Sandvik, Computational Studies of Quantum Spin Systems, *AIP Conference Proceedings* **1297**, 135 (2010), https://pubs.aip.org/aip/acp/article-pdf/1297/1/135/11407753/135_1.online.pdf.
- [90] Z.-Y. Lan, A.-L. He, and Y.-F. Wang, Flat bands with high chern numbers and multiple flat bands in multifold staggered-flux models, *Phys. Rev. B* **107**, 235116 (2023).
- [91] H. Dehghani, Z.-P. Cian, M. Hafezi, and M. Barkeshli, Extraction of the many-body chern number from a single wave function, *Phys. Rev. B* **103**, 075102 (2021).
- [92] H. Lu, H.-Q. Wu, B.-B. Chen, and Z. Y. Meng, From a fractional quantum anomalous hall state to a smectic state with equal hall conductance (2024), arXiv:2404.06745 [cond-mat.str-el].
- [93] D. N. Sheng, A. P. Reddy, A. Abouelkomsan, E. J. Bergholtz, and L. Fu, Quantum anomalous hall crystal at fractional filling of moiré superlattices (2024), arXiv:2402.17832 [cond-mat.mes-hall].
- [94] B. Andrews, T. Neupert, and G. Möller, Stability, phase transitions, and numerical breakdown of fractional chern insulators in higher chern bands of the hofstadter model, *Phys. Rev. B* **104**, 125107 (2021).
- [95] H. Li and F. D. M. Haldane, Entanglement spectrum as a generalization of entanglement entropy: Identification of topological order in non-abelian fractional quantum hall effect states, *Phys. Rev. Lett.* **101**, 010504 (2008).
- [96] A. Abouelkomsan, A. P. Reddy, L. Fu, and E. J. Bergholtz, Band mixing in the quantum anomalous hall regime of twisted semiconductor bilayers, *Phys. Rev. B* **109**, L121107 (2024).
- [97] H. Liu, K. Yang, A. Abouelkomsan, Z. Liu, and E. J. Bergholtz, Broken symmetry in ideal chern bands (2024), arXiv:2402.04303 [cond-mat.str-el].
- [98] H. Li, Y. Su, Y. B. Kim, H.-Y. Kee, K. Sun, and S.-Z. Lin, Contrasting twisted bilayer graphene and transition metal dichalcogenides for fractional chern insulators: an emergent gauge picture (2024), arXiv:2402.02251 [cond-mat.mes-hall].
- [99] M. Haque, O. S. Zozulya, and K. Schoutens, Entanglement between particle partitions in itinerant many-particle states, *Journal of Physics A: Mathematical and Theoretical* **42**, 504012 (2009).
- [100] B. A. Bernevig and F. D. M. Haldane, Model fractional quantum hall states and jack polynomials, *Phys. Rev. Lett.* **100**, 246802 (2008).
- [101] A.-L. He, W.-W. Luo, Y.-F. Wang, and C.-D. Gong, Fractional chern insulators in singular geometries, *Phys. Rev. B* **99**, 165105 (2019).
- [102] B. A. Bernevig and N. Regnault, Thin-torus limit of fractional topological insulators (2012), arXiv:1204.5682 [cond-mat.str-el].
- [103] G. Shavit and Y. Oreg, Quantum geometry and stabilization of fractional chern insulators far from the ideal limit (2024), arXiv:2405.09627 [cond-mat.str-el].
- [104] X. Shen, C. Wang, R. Guo, Z. Xu, W. Duan, and Y. Xu, Stabilizing fractional chern insulators via exchange interaction in moiré systems (2024), arXiv:2405.12294 [cond-mat.str-el].
- [105] B. Andrews, M. Raja, N. Mishara, M. P. Zaletel, and R. Roy, Stability of fractional chern insulators with a non-landau level continuum limit (2024), arXiv:2310.05758 [cond-mat.str-el].
- [106] B. Andrews and G. Möller, Stability of fractional chern insulators in the effective continuum limit of harper-hofstadter bands with chern number $|c| > 1$, *Phys. Rev. B* **97**, 035159 (2018).
- [107] Y.-H. Wu, J. K. Jain, and K. Sun, Fractional topological phases in generalized hofstadter bands with arbitrary chern numbers, *Phys. Rev. B* **91**, 041119 (2015).
- [108] C. H. Lee, R. Thomale, and X.-L. Qi, Pseudopotential formalism for fractional chern insulators, *Phys. Rev. B* **88**, 035101 (2013).
- [109] K. Yang, Y. Liu, F. Schindler, and C.-X. Liu, Engineering miniband topology via band-folding in moiré superlattice materials (2024), arXiv:2405.13145 [cond-mat.mes-hall].
- [110] G.-Y. Zhu, T. Xiang, and G.-M. Zhang, Spin-valley antiferromagnetism and topological superconductivity in the trilayer graphene moire super-lattice (2018), arXiv:1806.07535 [cond-mat.str-el].
- [111] G.-Y. Zhu, T. Xiang, and G.-M. Zhang, Inter-valley spiral order in the mott insulating state of a heterostructure of trilayer graphene-boron nitride, *Science Bulletin* **63**, 1087 (2018).